*Desalination and Water Treatment*
www.deswater.com
doi: 10.1080/19443994.2015.1028457

57 (2016) 9488–9497
April

Taylor & Francis
Taylor & Francis Group

# Fabrication and characterization of Ag-doped titania: impact of dye-sensitization, phenol decomposition kinetics and biodegradability index

Amit Kumar Behera, Ch Venkatanarasimha Rao, Raj Kumar Das, Ardhendu Sekhar Giri, Animes Kumar Golder*

*Department of Chemical Engineering, Indian Institute of Technology Guwahati, Assam 781 039, India, Tel. +91 9438632360; email: amitpunkster@gmail.com (A.K. Behera), Tel. +91 361 2582300; emails: venkata.rao@iitg.ernet.in (Ch.V. Rao), rkdas@iitg.ac.in (R.K. Das), a.giri@iitg.ernet.in (A.S. Giri), Tel. +91 361 258 2269; Fax: +91 361 258 2292; email: animes@iitg.ernet.in (A.K. Golder)*

Received 16 July 2014; Accepted 8 March 2015

ABSTRACT

Heterogeneous photocatalytic wastewater treatment using $TiO_2$ is a well-accepted technique under UV light illumination. Different strategies are employed to modify $TiO_2$ for shifting its photo-response to the visible light. In this work, Ag-doped $TiO_2$ nano-composites were synthesized by UV photo-reduction method to narrow down the band gap energy. Further, dye sensitization was performed using Eosin Yellowish to find out its influence on phenol decomposition. Synthesized catalysts were characterized using diffuse UV–vis spectroscopy, Fourier transform infrared spectroscopy, X-ray diffraction, transmission electron microscopy (TEM), Brunner Emmer Teller (BET) area and zeta-potential measurements. Nanowire like structure was observed with 30–70 nm in diameter from TEM images. BET surface area was decreased considerably with Ag-doping (maximum 31.6%) and dye sensitization (40.6%). Ag concentration and solution pH showed dramatic impact on phenol decomposition with maximum 87% at pH 7, Ag-loading 1% (w/w) and catalyst dose 0.5 g $L^{-1}$. Practically no positive synergy was noted with dye sensitization even though the photo-responses were moved intensely to the visible region. The pseudo-first order kinetic exhibited sound agreement to the experimental results with correlation coefficient ≥0.98. Moreover, the enhancement of biodegradability is investigated in terms of biochemical to chemical oxygen demand.

*Keywords:* Photo-catalyst; Ag-doping; Dye-sensitization; Phenol degradation

## 1. Introduction

Phenol and phenol-derivatives are common in various industrial effluents such as coal gasification [1], olive oil production [2] and petrochemicals [3]. Activated sludge process gives inefficient degradation of phenol and phenol derivatives due to toxic and inhibitory effects to microorganisms [4,5]. Phenolic effluent is usually characterized by low biochemical oxygen demand to chemical oxygen demand (BOD/COD) [6].

Advanced oxidation processes (AOPs) are most attractive for the decomposition of phenolic compounds [6,7]. AOPs take place both in homogeneous and heterogeneous reacting systems, in light and dark [8]. The common features of all the processes are generation

*Corresponding author.

of highly reactive hydroxyl free radicals ($HO^{\bullet}$). It causes consecutive unselective degradation of organic compounds leading to complete mineralization [9].

In heterogeneous photo-catalytic processes, light energy is employed to excite semiconductor materials, used as photo-catalyst, to produce electron/hole ($e^-/h^+$) pair [10,11]. The most common photo-catalyst is titania ($TiO_2$) for water decontamination studies [9]. The main advantages of $TiO_2$ photo-catalysis are: (i) treatment can be performed at ambient condition, (ii) hydroxyl radical ($HO^{\bullet}_{ad}$) formed could cause complete mineralization, and (iii) catalyst is less expensive, non-hazardous, stable and reusable [12]. However, $TiO_2$ is proven to be effective in UV light and only 5% of solar spectrum is available in the band gap energy of $TiO_2$. It implies that typically about 0.04% of solar photon is effective in $TiO_2$ photo-catalytic reaction considering the collector efficiency of 75% and catalyst efficiency of 1% [13]. Nevertheless about 40% of the sunlight is in the visible range (400–700 nm). Numerous efforts have been made to improve the photo-responses of $TiO_2$ in visible light. It includes doping with metal and non-metal materials or combining with another semiconductor of lower band gap energy [14,15]. Dye-sensitization of $TiO_2$ is another technique in which the catalyst is sensitized to the visible region with the help of a pre-adsorbed dye. Excited dye molecules upon illumination of visible light insert electron into the conduction band of $TiO_2$. However, dye-sensitization process suffers from rapid recombination of $e^-/h^+$ pair leading to poor catalyst activation [10]. Various dyes, namely, Eosin Y [10], porphyrin–Cu(II) [16], N719 [17], etc. have been used to change the spectral responses of $TiO_2$. Dye sensitized metal-doped $TiO_2$ is usually employed for simultaneous $H_2$ generation by water splitting and decomposition of organic materials [10]. However, there is lack of information on the role of dye sensitization over metal-doped $TiO_2$ for the degradation of contaminants.

A study is undertaken to uncover the necessity of dye sensitization of Ag-doped $TiO_2$ employing Eosin Y (EY), an anionic dye, for phenol degradation. The main objectives are to (i) synthesize Ag-doped $TiO_2$ ($TiO_2$/Ag) by photo-reduction method, (ii) sensitize $TiO_2$/Ag using EY ($TiO_2$/Ag/EY), (iii) characterize fabricated catalyst using Brunner Emmer Teller (BET), Fourier transform infrared spectroscopy (FTIR), solid-UV/Vis spectroscopy, TEM, X-ray diffraction (XRD) and zeta-potential analyses, and (iv) study the photo-catalyst activity in terms of phenol decomposition.

## 2. Materials and methods

### 2.1. Reagents

Eosin yellow (EY) dye (90% w/w purity) was obtained from Loba Chemie Pvt. Ltd., Mumbai. $AgNO_3$ (99% w/w purity), KBr (99.5% w/w purity) and $H_2SO_4$ (99% v/v purity) were procured from Merck, India. Titanium dioxide (99.5% w/w purity), NaOH pellets (99% w/w purity), and ethanol (98% v/v purity) were purchased from Changshu Yangyuan Chemical, China. Deionized water (DI) (Millipore, USA, model: Elix-3) was used to prepare all solutions and reagents.

### 2.2. Analytical techniques

Solid UV–vis spectrophotometer of Shimadzu, Japan (model: Solid Spec 3700/3700DUV) was employed to acquire the spectral absorbance of synthesized catalysts. FTIR spectra were obtained using FTIR spectrometer of Shimadzu, Japan (model: IR affinity-1). KBr salt was dried at 110°C for 2 h and the sample at 99:1 (w/w) was mixed in a mortar and pestle to record the spectra. XRD pattern was obtained between $2\theta$ angle from 10° to 80° (Bruker, Germany, model: D8 Advance). BET surface area was measured using BET instrument of Beckman Coulter, Switzerland (model: SA 3100). Morphology and size of catalyst particles were recorded using transmission electron microscope (JEOL, USA, model: JEM 2100). 0.2 g catalyst was suspended in 50 mL acetone and dispersed in an ultrasonic bath (Jeiotech Instruments, Korea, model: UC-02) for 20 min to separate individual particles. Zeta-potential measurement was performed using Zeta-potential analyser of Beckman Coulter, Switzerland (model: Delsa Nano-C particle analyzer). Suspended catalyst was separated out by filtration using 0.2 μm filter (Axiva Sichem Biotech, India, model: C-129M) and pH was recorded before zeta-potential measurement.

Phenol concentration was determined by colorimetric method using a UV–vis Spectrophotometer of Thermo Scientific, India (model: UV 2300). COD was found out using closed reflux titration method. A COD digester of HACH, USA (model: DRB 200) was used for sample digestion. BOD was obtained following the standard method [18]. Solution pH was measured using a precision pH meter of Eutech Instruments, Malaysia (model: pH/ion 510).

### 2.3. Catalyst synthesis

Ag-doped $TiO_2$ ($TiO_2$/Ag) nano crystals were synthesized by photo-reduction method. 10.008 g of $TiO_2$ was dispersed in an aqueous ethanol solution (ethanol/water = 30/270 v/v) with 0.027 g of $AgNO_3$ to obtain Ag-loading of 0.25% (w/w). Similarly, different amount of $AgNO_3$ was added into $TiO_2$/ethanol–water dispersion to synthesize $TiO_2$/Ag at weight percentage of 0.5, 0.75, 1 and 2. pH of $TiO_2$/$AgNO_3$ suspension was adjusted to 3 using 0.1 N $H_2SO_4$ and dispersed for 30 min in the ultrasonic bath. The suspension was left for 12 h in dark and then irradiated under a 160 W high pressure mercury lamp of Starlite (model: E27, India) for 2 h at 50 rpm on a magnetic stirrer (stirrer bar: length 40 mm, $\phi$ 0.8 mm) of Tarsons, India (model: Spinnot) for the reduction of $Ag^+$ into $Ag^0$. $TiO_2$/Ag particles were separated out by centrifugation (Remi, Mumbai, model: R-23) at 5,000 rpm for 30 min and washed with DI water. It was then dried for 12 h at 100°C in the hot air oven and grinded in the mortar and pestle. The fabricated $TiO_2$/Ag was stored in dark air tight container till characterization and catalyst activity test.

Dye sensitization of $TiO_2$/Ag-1.0 was carried out with 10 g in 200 mL EY solution (100 mg $L^{-1}$) with gentle stirring at 50 rpm for 12 h in dark. Catalyst particles were filtered out and washed with anhydrous ethanol to remove loosely adsorbed dye, if any. It was then dried at 100°C for 12 h and kept in dark to avoid catalyst de-activation. EY sensitized $TiO_2$/Ag-1.0 is designated as $TiO_2$/Ag-1.0/EY.

### 2.4. Phenol decomposition experiment

A cylindrical borosilicate glass vessel (1 L) was used as the reactor in batch mode. Experiment was carried out with 400 mL phenol solution at a fixed catalyst dose. pH was adjusted using 0.1 N $H_2SO_4$ and/or NaOH. Catalyst was dispersed in the test solution in the ultrasonic bath for 10 min and it was then kept in dark for 60 min to equilibrate phenol adsorption. A sample of about 5 mL was taken to determine the initial phenol concentration prior to illumination of light. Catalyst particles were separated by filtration. A visible lamp of 200 W (Bajaj, India) equipped on the top of the reactor (about 20 cm above solution) was used for reaction [12]. The solution was agitated at 100 rpm on the magnetic stirrer. The temperature was maintained at 25 ± 2°C with suitable cooling arrangement. Intermediate samples were withdrawn, catalyst particles were separated out and clear liquid was analyzed for phenol concentration. COD and BOD were determined at the end of experimental run (after 3 h) as both phenol and its oxidation products namely, cresol, hydroquinone and p-benzoquinone are toxic in nature [19,20].

## 3. Results and discussion

### 3.1. Catalyst characterization

#### 3.1.1. Spectral absorbance of synthesized $TiO_2$/Ag and $TiO_2$/Ag–EY

The enhanced photocatalytic activity of $TiO_2$ by Ag deposition is due to enhancement of $e^-/h^+$ separation and subsequent transfer of trapped electron to adsorbed $O_2$ acting as an acceptor [17]. Fig. 1 shows the spectral responses of synthesized Ag-doped titania. Ag-doping gradually increased the absorbance in the visible region with Ag-loading from 0.25 to 1% (w/w). The number of active sites could capture photo generated electron probably fell down with further increase in Ag percentage i.e. for 1.5 and 2% (w/w) Ag-doping [21]. EY sensitized Ag-doped $TiO_2$ ($TiO_2$/Ag-1.0/EY) showed the highest absorbance with a maxima at 450 nm due to dye coloration. The improvement in absorbance of EY sensitized $TiO_2$ ($TiO_2$/EY) (Fig. 1) was not as high as $TiO_2$/Ag-1.0/EY. It implies a better photoactivity of $TiO_2$/Ag-1.0/EY over $TiO_2$/EY in the visible wavelength of light.

#### 3.1.2. FTIR spectra

Infrared spectra provide important information on bonding nature of $TiO_2$ and EY dye by identifying the characteristic stretching frequencies. A strong broad

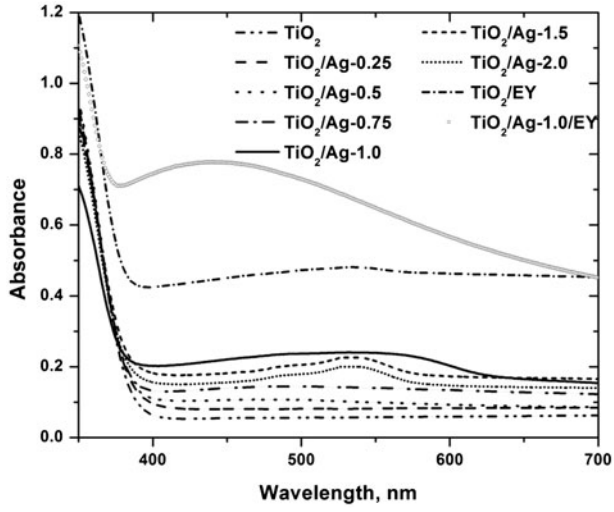


Fig. 1. Spectral absorption of fabricated photo-catalysts with wavelength.

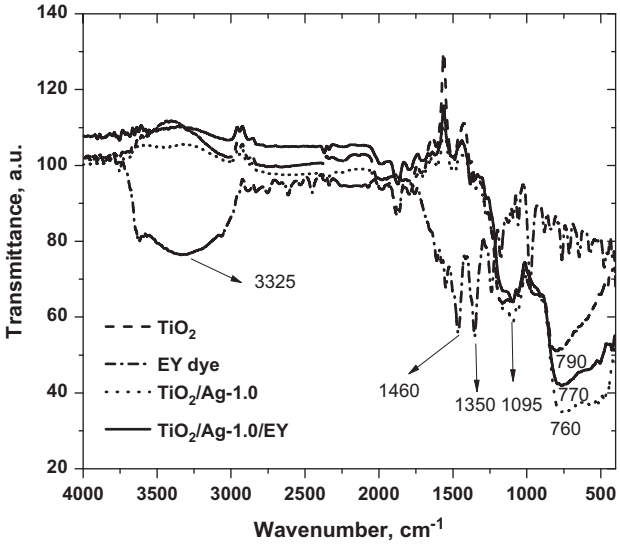


Fig. 2. FTIR spectra of bare $TiO_2$, EY and synthesized photo-catalysts.

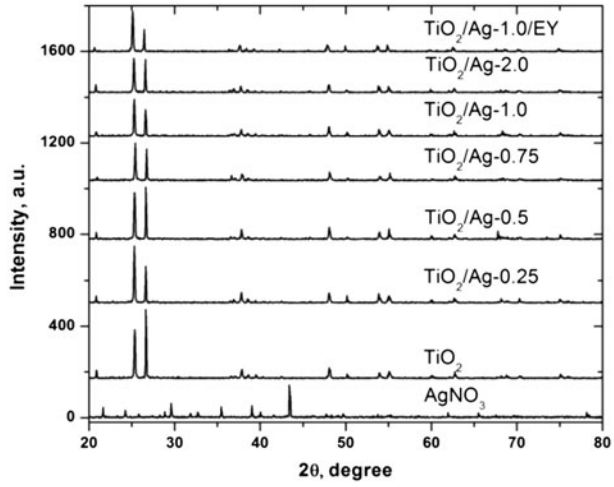


Fig. 3. XRD patterns of $AgNO_3$, $TiO_2$, and fabricated photo-catalysts.

band near 3,325 $cm^{-1}$ could be attributed to the stretching vibration of –OH group and interlayer water molecules (Fig. 2). This is mainly caused by Ti–O–H stretching vibration. The band near 1,460 $cm^{-1}$ can be allocated to bending vibration of H–O–H bond on $TiO_2$. Jeffrey and Cheng [22] reported that the band near 1,630 $cm^{-1}$ is due to bending vibration of H–O–H. It evidences formation of strong H-bond (H–O–H) due to surface adsorbed water and –OH groups. Ag-doping of $TiO_2$ increased surface-adsorbed water and –OH groups. Ti–O band was shifted from 790 to 760 $cm^{-1}$ because of asymmetrical stretching vibration of Ti–O–Ag. The evidence of EY adsorption on $TiO_2$ surface can be obtained by acquiring the vibrational spectra of EY molecules at the interface [23]. The band at 3,325 and 1,460 $cm^{-1}$ are assigned to –OH and C=O stretching of free –COOH and –OH groups. It completely disappeared after EY adsorption on $TiO_2$ suggesting EY adsorption on $TiO_2$ via its –COOH group. A broad band appeared at 1,350 $cm^{-1}$ can be assigned to scissoring mode of water molecule.

### 3.1.3. X-ray diffraction patterns

The XRD pattern of $AgNO_3$, $TiO_2$, $TiO_2$/Ag and $TiO_2$/Ag/EY were acquired to identify the crystalline phases. The results between $2\theta$ angles from 20° to 80° are shown in Fig. 3. The diffraction patterns were found to be similar to the crystal structure of $TiO_2$. $TiO_2$ showed both crystalline structures of anatase ($2\theta$ = 25.4°, 37.8°, 48.1°, 55.1°, 68.8°, 70.4°, 74.9°) and rutile ($2\theta$ = 26.7°, 36.5°, 54°, 62.9°) [24]. $TiO_2$/Ag and $TiO_2$/Ag/EY exhibited similar crystal structures of $TiO_2$. $Ag^+$ would bind with $TiO_2$ via an ion-exchange or coordination reaction [24]. It could function as a nucleation precursor thus the anatase and rutile phases are interchanged at 25.4° and 26.7° for 0.25% Ag loading as compared to bare $TiO_2$. However, the intensities of peaks at $2\theta$ = 25.4°, 26.7°, 37.8°, 48.1° and 55.1° reduced a bit with increase in Ag-loading from 0.5%. In fact, the XRD patterns did not follow any consistent trend with increasing Ag-loading. The intensity of two primary peaks at $2\theta$ = 25.4° and 26.7° correspond to anatase and rutile phases [25,26] reduced at higher Ag-loading (>5%). No phase transition was also observed. The characteristic peaks of Ag phase were not visible even for 1–2% of Ag-loading probably due to high its dispersion on $TiO_2$ [27,28].

### 3.1.4. TEM analysis

The shape and size of $TiO_2$/Ag-1.0/EY nanoparticles by TEM images are shown in Fig. 4. The composites appeared like nanowires with diameter size varying from 30 to 70 nm. The surface of $TiO_2$/Ag-1.0/EY nanoparticles was quite smooth and Ag-nanoparticles were uniformly deposited on $TiO_2$ surface. The close interconnections among the $TiO_2$/Ag-1.0/EY nanowires can be observed from TEM images. $TiO_2$/$Ag^0$ particles were probably formed at the beginning and $Ag^0$ could diffuse at the interfaces of $TiO_2$/$Ag^0$ segments due to generation of heat under UV light irradiation. Likewise nanowire-like structures were formed [29]. The Ag heads of nanowires were further connected leading to formation of nanowire network

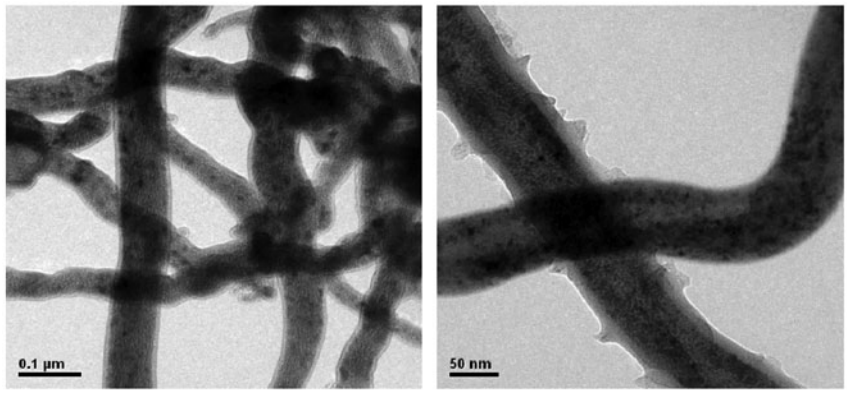


Fig. 4. TEM image of $TiO_2$/Ag-1.0/EY nanowires.

and, the interconnected nanowires could help the transfer and segregation of photo-generated $e^-/h^+$ pair [30].

#### 3.1.5. BET area

The catalyst samples were degassed at 200°C prior to $N_2$ adsorption. Ag-doping led to decrease in BET surface area from 15.77 to 9.36 $m^2\ g^{-1}$. Fig. 5 displays almost a linear reduction of BET surface area with different loading percentage of Ag. Photo-reduction of Ag probably would have compacted $TiO_2$ nano-particles. The surface area of $TiO_2$ decreased by about 31.6% with 1% Ag-loading and it was 40.6% with EY sensitization with respect to the raw $TiO_2$. A reference (or treated) $TiO_2$ was prepared following the same procedure of Ag-doping, however, without Ag to understand the effect of the procedure on BET area. Marginal change was noted for treated $TiO_2$ in comparison to raw $TiO_2$ (Fig. 5). Cheng et al. observed about 78% reduction in BET surface area of $TiO_2$ with Ag doping (pore volume 0.12) by vapor-thermal method [30]. Surface fluorination caused as high as 38% decrease in BET area of $TiO_2$ with atomic ratio of 1.0 [31].

#### 3.1.6. Zeta-potential (ζ)

The surface of $TiO_2$/Ag and $TiO_2$/Ag-1.0/EY particles is positively charged below the point of zero charge ($pH_{zpc}$) and carries negative charge above it. The variation of zeta-potential (ζ) of Ag-doped $TiO_2$ is shown in Fig. 6. ζ of bare $TiO_2$ varied 15 to −17.6 mV for pH from 4 to 8 with $pH_{zpc}$ of 6.3. The surface adsorbed −OH groups gave negatively charged surface of $TiO_2$ in the aqueous media [32]. It is also clearly supported by FTIR spectra. The surface becomes positively charged due to adsorption of proton (Eq. (1)) [33]. The value of ζ was more negative with increase in pH and similarly it became more positive with decrease in pH from $pH_{zpc}$. It varied from 6.1 to 6.4 with Ag-doped $TiO_2$. EY pre-adsorption did not much influence $pH_{zpc}$ but ζ showed strong dependency on pH at the same Ag-loading. It implies that EY pre-adsorption facilitated proton and $OH^-$ adsorption at lower and higher pH. The variation of ζ with $TiO_2$/Ag-1.0/EY was fairly similar to that of $TiO_2$/Ag-2.0. The negatively charged $TiO_2$/Ag and $TiO_2$/Ag-1.0/EY particles resist them from forming of aggregates due to electrostatic repulsion at higher pH. The stability of particles increases when the value of ζ is more negative [34] i.e. higher Ag-loaded and EY sensitized particles were more stable at higher pH. ζ varied from −18 to −38.5 mV at pH 8 signifying that the particles were well dispersed in aqueous medium. The same were found to be between 13 and 22 mV at pH 4 (Fig. 6). It implies that the synthesized $TiO_2$/Ag and $TiO_2$/Ag-1.0/EY particles opposed against destabilization at lower pH. As a result the value of ζ did not increase much at pH 4 compared to pH 8.

$$TiO_2 \equiv OH + H^+ \leftrightarrow TiO_2 \equiv OH_2^+ \quad (1)$$

### 3.2. Photo-activity of synthesized catalyst and determination of optimal condition for phenol decomposition

#### 3.2.1. Effect of Ag-loading in $TiO_2$ doping and EY sensitization for phenol degradation

The performance of synthesized Ag-doped $TiO_2$ with Ag-loading and EY sensitization for phenol decomposition is shown in Fig. 7. It was found that phenol degradation under visible light irradiation increased with Ag-loading up to 1% (w/w) starting from 0.25% (w/w). About 87% phenol degradation

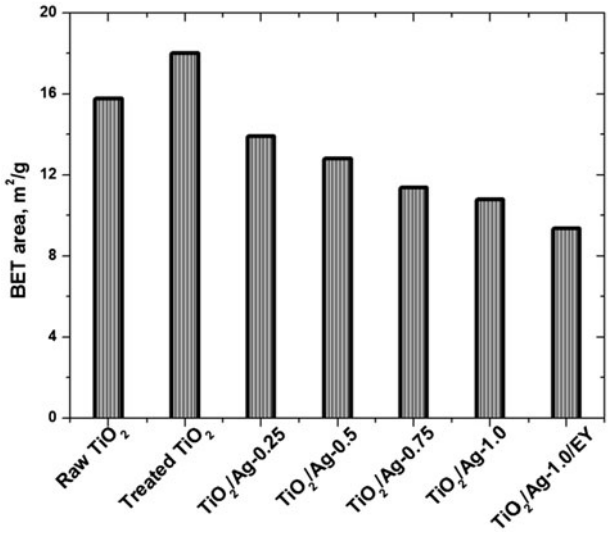


Fig. 5. BET area of Ag-doped and dye sensitized catalysts.

was achieved using $TiO_2$/Ag-1.0 against 53% with $TiO_2$/Ag-0.25. The reason is that Ag could enhance $e^-/h^+$ separation resulting in improved photocatalytic activity under visible light. It facilitates formation of ($O_2^{\cdot-}$) and ·OH by reacting with water and oxygen on the catalyst surface. Furthermore, it is in line with variation of absorbance (Fig. 1). However, lower phenol degradation 73% was achieved using $TiO_2$/Ag-2.0. Higher Ag-loading could enhance the recombination of $e^-/h^+$ pair. Dye sensitization of $TiO_2$/Ag-1.0 gave only 3% improvement in phenol degradation (Fig. 7). The value of LUMO energy level of dye is more negative than one of conduction band of $TiO_2$ as shown in Fig. 8. It implies that electron transfer to the conduction band initiated by dye sensitization under visible light illumination did not exhibit additional phenol decomposition with 1% (w/w) Ag-loading of $TiO_2$/Ag-1.0/EY. Hence, the subsequent studies were carried using $TiO_2$/Ag-1.0 and $TiO_2$/Ag-1.0/EY.

### 3.2.2. Effect of pH

Fig. 9 shows the effect of pH on phenol decomposition at the end of irradiation of 2 h. It was found that phenol degradation was about 2–7% more with $TiO_2$/Ag-1.0/EY for the pH from 3 to 7. $TiO_2$/Ag-1.0 superseded the performance $TiO_2$/Ag-1.0/EY at pH ≥9.0. The adsorption and degradation of phenol depends on the surface charge of synthesized catalyst. The amphoteric behaviour of $TiO_2$ nanoparticles influences the surface charge of the photocatalyst. pH of the solution mostly controls the surface charge [35] and could also shift the position of redox reaction [32]. The following two equilibriums could take place (Eqs. (2) and (3)) due to amphoteric nature of $TiO_2$.

$$Ti–OH + OH^- = Ti–O^- + H_2O \quad (2)$$

$$Ti–OH + H^+ = Ti–OH_2^+ \quad (3)$$

The surface of catalyst particle became positively charged in acidic medium and it is negatively charged at pH ≥ (6.1–6.4) (Fig. 6). EY would have strongly affinity to be adsorbed on the surface below $pH_{zpc}$ being anionic in nature. On the other way it implies that EY dye could not desorb from the catalyst surface. ·OH could react with proton at lower pH (Eq. (4)) forming hydronium cation which is resulted in lower phenol degradation. Lower phenol removal also may be because of reduction in color intensity of EY dye at this pH. Maximum phenol degradation was noted at pH 7 with both the catalysts. $TiO_2$/Ag-1.0/EY exhibited 90% removal against 87% with $TiO_2$/Ag-1.0. Higher pH caused desorption of EY and it eventually prevented the penetration of light into the solution due to coloration. Moreover, high pH could scavenge ·OH leading to lower phenol degradation. It is necessary to mention that EY dye could undergo self-sensitized degradation under visible light illumination (>420 nm) over the period of reaction time [36].

$$^{\cdot}OH + 2H^+ \leftrightarrow H_3O^+ \quad (4)$$

### 3.2.3. Effect of catalyst dosage

The effect of the amount of catalyst on the removal of phenol was found to be significant. The variation in phenol decomposition at different catalyst dosages was determined in the range of 0.1–0.9 g $L^{-1}$. The results are shown in Fig. 10. Removal efficiency rose with increase in concentration of catalyst and then it decreased after a limiting value. This is due to the fact that the increase in the number of $TiO_2$ particles increase the number of photons absorbed and consequently phenol degradation. Aggregation of free catalyst particles could occur at high catalyst concentration which was resulted in decrease in the number of active sites. Further, the excessive opacity and screening effect of $TiO_2$/Ag-1.0 and $TiO_2$/Ag-1.0/EY at high catalyst dose could hinder light penetrations. It decreases the available surface area for light harvesting. As a result the catalytic activity is reduced. There was a loss of 10% phenol degradation for both the catalysts with increase in dose from 0.5 to 0.9 g $L^{-1}$ i.e. with 80% more catalyst concentration.

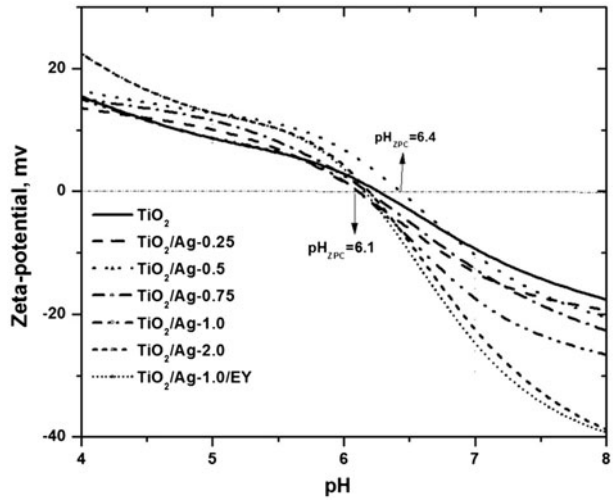


Fig. 6. Zeta-potential vs. pH of fabricated photo-catalysts.

### 3.2.4. Kinetics of phenol decomposition

It was found that the mass transfer effect on the kinetics of phenol decomposition was negligible at ≥100 rpm (results not shown). The rate of phenol degradation indeed followed the pseudo-first order kinetic model (Eq. (5)) (Fig. 7). The best fit parameters at various experimental conditions using the synthesized photocatalyst for phenol degradation are summarized in Table 1. The correlation coefficient ($R^2$) was found to be ≥0.98 for all the cases. The lowest rate constant ($k$) of $3.8 \times 10^{-3}$ min$^{-1}$ was determined with raw $TiO_2$ at pH 7 with 0.5 g L$^{-1}$. There was about

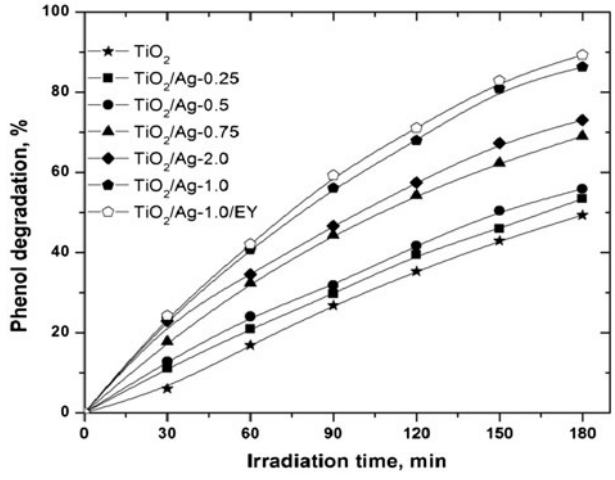


Fig. 7. Phenol degradation vs. irradiation time using synthesized catalysts. Catalyst 0.5 g L$^{-1}$, pH 7, [Phenol]$_0$ 20 mg L$^{-1}$, agitation speed 100 rpm and solution volume 400 mL.

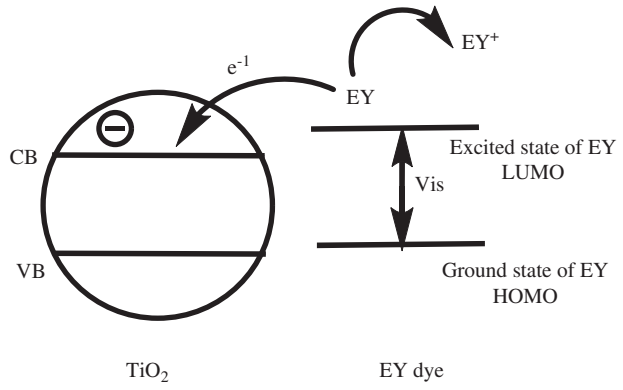


Fig. 8. Transition of electron from LUMO (dye) to CB of $TiO_2$.

2.8 to 3-fold increase in $k$ at pH 7 than the same at pH 3, 5 and 11 using $TiO_2$/Ag-1.0. The corresponding value of $k$ was $2.86 \times 10^{-3}$, $3.48 \times 10^{-3}$ and $2.39 \times 10^{-3}$ min$^{-1}$, respectively. The rate contact, $k$, was about 10% higher with $TiO_2$/Ag-1.0/EY than $TiO_2$/Ag-1.0 even though phenol decomposition only 3% more. The rate of phenol degradation using $TiO_2$/Ag-1.0 outperformed $TiO_2$/Ag-1.0/EY at pH ≥9 due to enhanced EY desorption. $k$ reduced by about 20 to 29% at pH 9 and 11 with $TiO_2$/Ag-1.0/EY. However, the rate was always faster with $TiO_2$/Ag-1.0/EY at different catalyst doses (0.1–0.9 g L$^{-1}$) at pH 7. Antonopoulou and Konstantinou [37] obtained the similar results for $k$ as $1.08 \times 10^{-3}$ min$^{-1}$ with $TiO_2$ dose of 0.1 g/L at 40 min under simulated solar irradiation. Abdullah et al. [38] reported that solar light activated $TiO_2$ process exhibited the rate constant of $3.37 \times 10^{-3}$ and $1.42 \times 10^{-3}$ min$^{-1}$ for the decomposition of phenol red and Rhodamine 6G, respectively, at neutral pH. The pseudo-first order $k$ well matched with the present work for the degradation of ethyl orange dye using $TiO_2$ (99.9% anatase) and a high pressure mercury lamp under aerobic condition [39]. They found that $k$ varied from $1.1 \times 10^{-3}$ to $7.8 \times 10^{-3}$ min$^{-1}$ at various pHs (2–11).

$$C_{\text{phenol}} = C^0_{\text{phenol}} \exp(-kt) \quad (5)$$

### 3.3. Biodegradability

$BOD_5$/COD ratio is a significant indicator to study the biodegradability nature of organic contaminants. The contaminated effluent is easily biodegradable when subjected to biological treatment with $BOD_5$/COD ≥ 0.4 [40]. Phenol is relatively non-biodegradable in nature and $BOD_5$/COD ratio of 0.18 was found

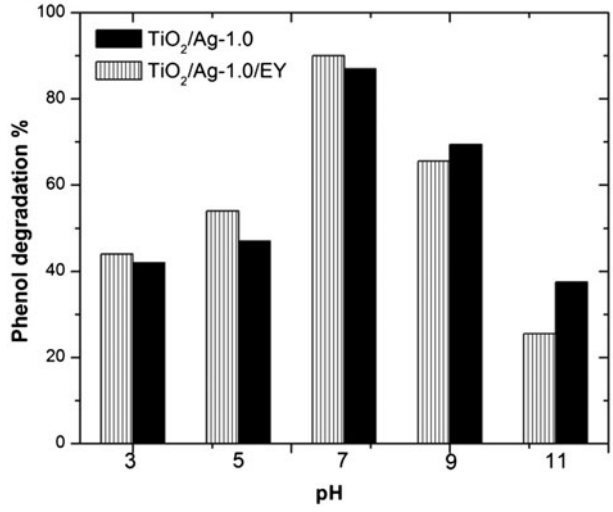


Fig. 9. Phenol degradation with solution pH. Irradiation time 2 h, Catalyst 0.5 g $L^{-1}$, $[Phenol]_0$ 20 mg $L^{-1}$, agitation speed 100 rpm and solution volume 400 mL.

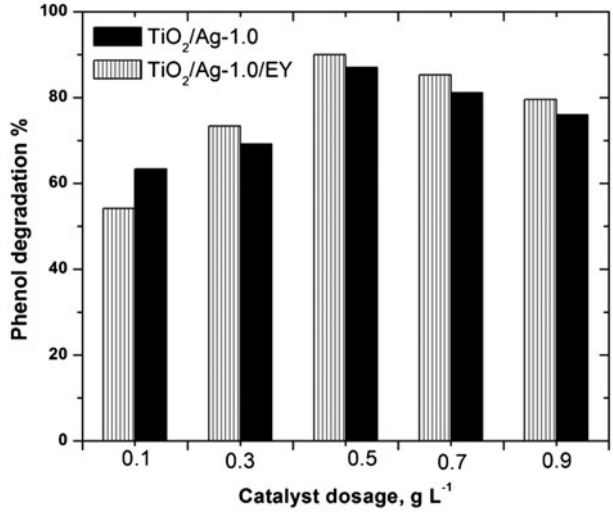


Fig. 10. Phenol degradation with catalyst dose. Irradiation time 2 h, $[Phenol]_0$ 20 mg $L^{-1}$, pH 7, agitation speed 100 rpm and solution volume 400 mL.

with 20 mg $L^{-1}$ phenol ($BOD_5$ 10 and COD 55 mg $L^{-1}$). Partial oxidation could yield more biodegradable products together with the destruction of inhibitory effect towards microorganisms in the downstream biological treatment. It also increases the overall treatment efficiencies compared to the efficiency of individual process.

The biodegradability index increased up to 0.55 and 0.65 after 2 h of visible light irradiation at pH 7 with 0.5 g $L^{-1}$ catalyst using $TiO_2$/Ag-1.0 and

Table 1
Kinetic parameters of phenol decomposition using synthesized catalysts

| Catalyst | Catalyst dose (g $L^{-1}$) | pH | $k \times 10^3$ ($min^{-1}$) | $R^2$ |
|---|---|---|---|---|
| $TiO_2$ | 0.5 | 7 | 3.8 | 0.99 |
| $TiO_2$/Ag-0.25 | 0.5 | 7 | 3.9 | 0.99 |
| $TiO_2$/Ag-0.5 | 0.5 | 7 | 4.14 | 0.99 |
| $TiO_2$/Ag-0.75 | 0.5 | 7 | 6.51 | 0.99 |
| $TiO_2$/Ag-1.0 | 0.1 | 7 | 3.89 | 0.98 |
| | 0.3 | 7 | 5.98 | 0.98 |
| | 0.5 | 7 | 10.67 | 0.99 |
| | 0.7 | 7 | 9.05 | 0.98 |
| | 0.9 | 7 | 7.73 | 0.98 |
| | 0.5 | 3 | 2.86 | 0.99 |
| | 0.5 | 5 | 3.48 | 0.98 |
| | 0.5 | 9 | 6.56 | 0.99 |
| | 0.5 | 11 | 2.39 | 0.98 |
| $TiO_2$/Ag-2.0 | 0.5 | 7 | 6.56 | 0.99 |
| $TiO_2$/Ag-1.0/EY | 0.1 | 7 | 4.83 | 0.98 |
| | 0.3 | 7 | 6.89 | 0.99 |
| | 0.5 | 7 | 11.8 | 0.99 |
| | 0.7 | 7 | 10.16 | 0.98 |
| | 0.9 | 7 | 8.33 | 0.98 |
| | 0.5 | 3 | 3.08 | 0.99 |
| | 0.5 | 5 | 4.29 | 0.99 |
| | 0.5 | 9 | 5.23 | 0.98 |
| | 0.5 | 11 | 1.69 | 0.99 |

$TiO_2$/Ag-1.0/EY, respectively. It implies that treated phenolic effluent is amicable for subsequent biological treatment. Ksibi et al. [40] reported the increase in biodegradability index from 0.05 to 0.56 for different substituted phenols after UV/$TiO_2$ treatment. $BOD_5$/COD of an industrial phenolic wastewater increased from 0.2 to 0.5 after 240 min of reaction with immobilized $TiO_2$ nano particles [41]. Both $TiO_2$/Ag-1.0 and $TiO_2$/Ag-1.0/EY also were as effective as photocatalytic ozonation of phenolic wastewater using UVA/$TiO_2$ [42].

## 4. Conclusions

Ag-doped $TiO_2$ nano-composites and dye sensitized $TiO_2$ photo-catalyst were successfully synthesized. The highest spectral absorbance was recorded at 447 nm in case of EY sensitized $TiO_2$ with 1% (w/w) Ag-loading against the same at 535 nm with Ag-doping only. Both Ag-doping and EY sensitization reduced the BET surface area of $TiO_2$ resulted from $TiO_2$ nanowire interconnections. Zeta-potential was more dependent on pH over a wide range at higher concentration of dopant metal as well as with EY sensitization. Solution pH had significant effect on the adsorption–desorption characteristics of phenol and for its subsequent degradation. Maximum phenol degradation took place at pH 7. The concentration of Ag and catalyst dose gave highest phenol degradation were of 1% (w/w) and 0.5 g $L^{-1}$. Careful optimization of dopant metal concentration would overcome the need of dye sensitization and; it is only important when hydrogen generation is considered. EY sensitization marginally improved (max 3%) phenol degradation under visible light. The pseudo first order rate constant was determined at different pH and catalyst dosages and it varied from $1.69 \times 10^{-3}$ $min^{-1}$ to as high as $11.8 \times 10^{-3}$ $min^{-1}$. The initial biodegradability index of 20 mg $L^{-1}$ was found to be 0.18. It increased to 0.55 and 0.65 when 1% (w/w) Ag-doped $TiO_2$ without and with EY sensitization was used for phenol decomposition.

## References

[1] F. Fang, H. Han, Q. Zhao, Chunyan Xu, L. Zhang, Bioaugmentation of biological contact oxidation reactor (BCOR) with phenol-degrading bacteria for coal gasification wastewater (CGW) treatment, Bioresour. Technol. 150 (2013) 314–320.

[2] L. Martirani, P. Giardina, L. Marzullo, G. Sannia, Reduction of phenol content and toxicity in olive oil mill waste waters with the ligninolytic fungus plueorotus ostreatus, Water Res. 30(8) (1995) 1914–1918.

[3] Ł. Chrzanowski, M. Owsianiak, A. Szulc, R. Marecik, A. Piotrowska-Cyplik, A.K. Olejnik-Schmidt, J. Staniewski, P. Lisiecki, F. Ciesielczyk, T. Jesionowski, H.J. Heipieper, Interactions between rhamnolipid biosurfactants and toxic chlorinated phenols enhance biodegradation of a model hydrocarbon-rich effluent, Int. Biodeterior. Biodegrad. 65 (2011) 605–611.

[4] G. Moussavi, A. khavanin, R. Alizadeh, The integration of ozonation catalyzed with MgO nanocrystals and the biodegradation for the removal of phenol from saline wastewater, Appl. Catal., B 97 (2010) 160–167.

[5] B. Marrot, A. Barrios-Martinez, P. Moulin, N. Roche, Biodegradation of high phenol concentration by activated sludge in an immersed membrane bioreactor, Biochem. Eng. J. 30 (2006) 174–183.

[6] Z. Zeng, H. Zou, X. Li, M. Arowo, B. Sun, J. Chen, G. Chu, L. Shao, Degradation of phenol by ozone in the presence of Fenton reagent in a rotating packed bed, Chem. Eng. J. 229 (2013) 404–411.

[7] O.B. Ayodele, J.K. Lim, B.H. Hameed, Degradation of phenol in photo-Fenton process by phosphoric acid modified kaolin supported ferric-oxalate catalyst: Optimization and kinetic modeling, Chem. Eng. J. 197 (2012) 181–192.

[8] N.M. Fadzil1, Z. Zainal, A.H. Abdullah, Ozone-assisted decolorization of methyl orange via homogeneous and heterogeneous photocatalysis, Int. J. Electrochem. Sci. 7 (2012) 11993–12003.

[9] A.S. Giri, A.K. Golder, Fenton, photo-Fenton, $H_2O_2$ Photolysis, and $TiO_2$ photocatalysis for dipyrone oxidation: Drug removal, mineralization, biodegradability, and degradation mechanism, Ind. Eng. Chem. Res. 53(4) (2014) 1351–1358.

[10] P. Chowdhury, J. Moreira, H. Gomaa, A.K. Ray, Visible-solar-light-driven photocatalytic degradation of phenol with dye-sensitized $TiO_2$: Parametric and kinetic study, Ind. Eng. Chem. Res. 51(12) (2012) 4523–4532.

[11] A.S. Giri, A.K. Golder, Ciprofloxacin degradation from aqueous solution by Fenton oxidation: Reaction kinetics and degradation mechanisms, RSC Adv. 4(13) (2014) 6738–6745.

[12] N. Riaz, F.K. Chong, Z.B. Man, M.S. Khan, B.K. Dutta, Photodegradation of orange II under visible light using Cu–Ni/$TiO_2$: Influence of Cu:Ni mass composition, preparation, and calcination temperature, Ind. Eng. Chem. Res. 52 (2013) 4491–4503.

[13] J. Zhang, Yongmei Wu, Mingyang Xing, S.A. Leghari, Development of modified N doped $TiO_2$ photocatalyst with metals, nonmetals and metal oxides, Energy Environ. Sci. 3 (2010) 715–726.

[14] O. Teruhisa, M. Akiyoshi, T. Umebayashi, K. Asai, T. Mitsui, M. Matsumura, Preparation of S-doped $TiO_2$ photocatalysts and their photocatalytic activities under visible light, Appl. Catal., A 265 (2004) 115–121.

[15] R. Liu, P. Wang, X. Wang, H. Yu, J. Yu, UV- and visible-light photocatalytic activity of simultaneously deposited and doped Ag/Ag(I)–$TiO_2$ photocatalyst, J. Phys. Chem. C 116 (2012) 17721–17728.

[16] Zhi-Li Ma, Gui-Fang Huang, Dong-Sheng Xu, Ming-Gang Xia, Wei-Qing Huang, Y. Tian, Coupling effect of La doping and porphyrin sensitization on photocatalytic activity of nanocrystalline $TiO_2$, Mater. Lett. 108 (2013) 37–40.

[17] T.C. Wang, L.H. Sio, Improving photovoltaic performance of titanium oxide thin films by integration of iron doping and dye sensitization, Surf. Coat. Technol. 244 (2014) 63–68.
[18] APHA, Standard Methods for the Examination of Water and Wastewater, 20th ed., American Public Health Association, Washington, 1998.
[19] A. Rubalcaba, M.E. Suárez-Ojeda, F. Stüber, A. Fortuny, Phenol wastewater remediation: Advanced oxidation processes coupled to a biological treatment, Water Sci. Technol. 55 (2007) 221–227.
[20] R. Alnaizy, A. Akgerman, Advanced oxidation of phenolic compounds, Adv. Environ. Res. 4 (2000) 233–244.
[21] T.D. Pham, B.K. Lee, Feasibility of silver doped $TiO_2$/glass fiber photocatalyst under visible irradiation as an indoor air germicide, Int. J. Environ. Res. Pub. Health 11 (2014) 3271–3288.
[22] C.W. Jeffrey, Y.T. Cheng, In situ FTIR study of photocatalytic NO reaction on photocatalysts under UV irradiation, J. Catal. 237 (2006) 393–404.
[23] Z. Fan, S. Feng, M. Wei, G. Fei, J. Yang, L. Hui, W. Jingchuan, S. Xinyan, L. Xinghua, M. Sheng, Controlling adsorption structure of eosin Y dye on nanocrystalline $TiO_2$ films for improved photovoltaic performances, J. Phys. Chem. C 117 (2013) 14659–14666.
[24] W. Li, C. Liang, W. Zhou, J. Qiu, Z. Zhou, G. Sun, Q. Xin, Preparation and characterization of multiwalled carbon nanotube-supported platinum for cathode catalysts of direct methanol fuel cells, J. Phys. Chem. B 107 (2003) 6292–6299.
[25] A. Maurizio, B. Mrianna, P. Agatino, P. Leonardo, Preparation and photoactivity of nanostructured anatase, rutile and brookite $TiO_2$ thin films, Chem. Commun. 47 (2006) 4943–4945.
[26] M. Xie, L. Jing, J. Zhou, J. Lin, H. Fu, Synthesis of nanocrystalline anatase $TiO_2$ by one-pot two-phase separated hydrolysis–solvothermal processes and its high activity for photocatalytic degradation of Rhodamine B, J. Hazard. Mater. 176 (2010) 139–145.
[27] T. Sreethawong, Y. Suzuki, S. Yoshikawa, Photocatalytic evolution of hydrogen over mesoporous $TiO_2$ supported NiO photocatalyst prepared by single-step sol–gel process with surfactant template, Int. J. Hydrogen Energy 30 (2005) 1053–1062.
[28] H. Zhu, Y. Wu, X. Zhao, H. Wan, L. Yang, J. Hong, Q. Yu, L. Dong, Y. Chen, C. Jian, J. Wei, P. Xu, Influence of impregnation times on the dispersion of CuO on anatase, J. Mol. Catal. A: Chem. 243 (2006) 24–30.
[29] Z. Gu, H. Ye, A. Bernfeld, K.J.T. Livi, D.H. Gracias, Three-dimensional electrically interconnected nanowire networks formed by diffusion bonding, Langmuir 23 (2007) 979–982.
[30] B. Cheng, Yao Le, Jiaguo Yu, Preparation and enhanced photocatalytic activity of Ag@$TiO_2$ core–shell nanocomposite nanowires, J. Hazard. Mater. 177 (2010) 971–977.
[31] Y. Jiaguo, W. Wenguang, B. Cheng, Bao-Lian Su, Enhancement of photocatalytic activity of mesporous $TiO_2$ powders by hydrothermal surface fluorination treatment, J. Phys. Chem. C 113 (2009) 6743–6750.
[32] I.K. Konstantinou, T.A. Albanis, $TiO_2$-assisted photocatalytic degradation of azo dyes in aqueous solution: Kinetic and mechanistic investigations, Appl. Catal., B 49 (2004) 1–14.
[33] G. Biresaw, K. Mittal, Surfactants in Tribology, vol. 3, CRC Press, Boca Raton, FL, 2013.
[34] P. Ionel, G. Graeme, P. Georg, B. Michal, Attractive electrostatic forces between identical colloidal particles induced by adsorbed polyelectrolytes, J. Phys. Chem. Lett. 113 (2009) 8458–8461.
[35] D. Mortada, B. Dalila, Water pH and surfactant addition effects on the stability of an Algerian crude oil emulsion, J. Saudi Chem. Soc. 16 (2012) 333–337.
[36] C. Debabrata, D. Shimanti, R.S. Dhodapkar, N.R. Nageswar, Simultaneous degradation of non-emissive and emissive dyes on visible light illuminated $TiO_2$ surface, J. Mol. Catal. A. Chem. 260 (2006) 264–268.
[37] M. Antonopoulou, I. Konstantinou, Photocatalytic treatment of metribuzin herbicide over $TiO_2$ aqueous suspensions: Removal efficiency, identification of transformation products, reaction pathways and ecotoxicity evaluation, J. Photochem. Photobiol. A: Chem. 294 (2014) 110–120.
[38] M.A. Abdullah, S.A. Muhammed, A.A. Tariq, D.A. Abdullah, Photodegradation of Rhodamine 6G and phenol red by nanosized $TiO_2$ under solar irradiation, J. Saudi Chem. Soc. 15 (2011) 121–128.
[39] M. Montazerozohori, S.M. Jahromi, Photocatalytic decolorization of ethyl orange at various buffer solutions using nano-titanium dioxide: A kinetic investigation, Desalin. Water Treat. 48 (2012) 261–266.
[40] M. Ksibi, A. Zemzemi, R. Boukchina, Photocatalytic degradability of substituted phenols over UV irradiated $TiO_2$, J. Photochem. Photobiol. A: Chem. 159 (2003) 61–70.
[41] M. Habibi, A.A.L. Zinatizadeh, M. Akia, Photocatalytic degradation of tire cord manufacturing wastewater using an immobilized nano $TiO_2$ photocatalytic reactor, Desalin. Water Treat. (2014), doi: 10.1080/19443994.2014.979328.
[42] O. Gimeno, A.L. Fernandez, M. Carbajo, F. Beltran, J. Rivas, Photocatalytic ozonation of phenolic wastewaters: Syringic acid, tyrosol and gallic acid, J. Environ. Sci. Health, A 43 (2008) 61–69.